Improved assistive profile tracking of soft exosuits for walking and jogging with off-board actuation

Giuk Lee*, *Member, IEEE*, Ye Ding*, Ignacio Galiana Bujanda, Nikos Karavas, Yu Meng Zhou, Conor J. Walsh, *Member, IEEE*

***Abstract*— In this paper, we present a design and control approach of a modular off-board actuation system with mono-articular hip exosuit, enabling the instantaneous assistive profile modification of magnitude, shape, and timing. The off-board system consists an actuation unit with two degrees of freedom that can transmit forces to our soft exosuit via Bowden cables. To perform accurate force tracking and cable slack management, we implemented a switching admittance-position control approach that utilizes the advantages of both admittance and position control. In particular, feedforward models (FFMs) are added to the admittance control to compensate variability of individual kinematics, nonlinear hip exosuit stiffness and actuator transmission loss to enable a more accurate force tracking. This system allows us to track force profiles accurately and robustly under normal walking or jogging speed. The performance of force tracking was evaluated on three subjects walking on a treadmill at 1.25 m/s with various magnitude, shape, and timings of assistive profiles and jogging on a treadmill at 2.3 m/s with varied magnitude of a representative assistance profile. Results showed that assistance could be delivered reliably across different profiles. In case of walking experiments, the errors of the magnitude, RMS-E, and timing were within 2.0 N, 8.4 N, and 1.8% when varying the magnitude, shape, and timing respectively. In case of jogging experiments, the RMS-E was within 3.0 N. This system will be used for future research examining how to individualize assistive profiles for different wearers during walking and jogging.**

I. Introduction

In the past decades, lower-limb exoskeletons have been drawing intense research interest because of their potential applications to assist or augment human performances for various purposes. Some of the exoskeletons are designed to support and train a paraplegic's body [1]–[7], while others improve the walking efficiency of able-bodied individuals, especially in case of load-carrying [8]–[11]. The majority of these devices consist of rigid structures, which are favorable for supporting the carried load or body weight and producing high assistive force to the wearer. However, the rigid nature can interfere natural movement of the wearer when the exoskeleton joints are misaligned with biological joints or the degree of freedom are not supported [12]–[14]. Moreover, the large inertia of rigid structures on the distal locations can significantly increase the wearer's net metabolic rate when they are not fully compensated [8]. Thus, many research groups, moved to a solution of lighter interfaces with more efficient actuation strategy to avoid the challenges of more traditional exoskeletons [15]–[17].

Our group's approach to mitigate the challenges associated with rigid exoskeletons, has been to develop "soft exosuits", that use functional apparel to provide a conformal, lightweight and non-restrictive means to interface to the wearer's body [18]–[20]. Combining the textile-based structure with Bowden cable actuation and force-based position control approaches we have demonstrated that we can deliver significant assistive forces to wearers without restricting their natural movement [21]–[23]. For portable systems, this approach enables the wearable robot to have low inertia on distal limb locations by having the actuation unit close to the wearer's center of the mass, thus minimizing the impact of the system on the wearer's energetics.

To explore the lower-limb assistance research with soft exosuits in an efficient and controlled manner, we previously developed reconfigurable off-board actuation platforms that can be used to assist one or more joints [19], [20], [22]. These platforms have the heavier actuation components removed from the wearer similar to [24]–[26] and enable a wide range of assistance strategies to be applied to the lower extremities without adversely affecting the natural dynamics of walking. We have demonstrated the utility of these platforms for

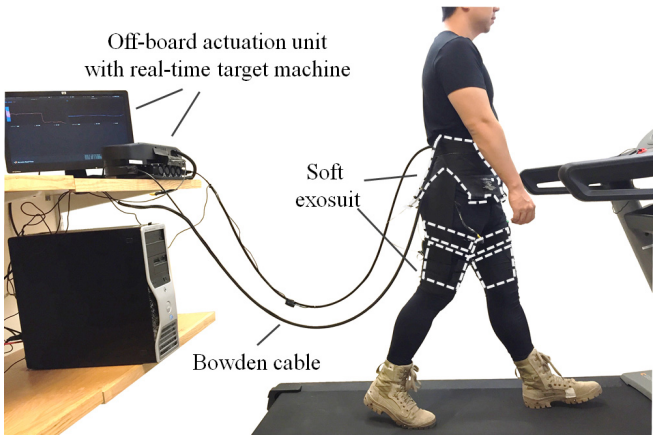

Figure 1. Overview of an off-board actuation platform with hip exosuit. The off-board actuation platform is shown on the left. Two sets of Bowden cables are connected to the soft exosuit to provide hip extension assistance during walking.

This material is based upon work supported by the Defense Advanced Research Projects Agency (DARPA), Warrior Web Program (Contract No. W911NF-14-C-0051). This work was also partially funded by the Wyss Institute for Biologically Inspired Engineering and the School of Engineering and Applied Sciences at Harvard University.

* - these authors contributed equally to the work

G. Lee (e-mail: giuklee@seas.harvard.edu), Y. Ding (e-mail: yding@seas.harvard.edu), I. Galiana (e-mail: ignacio.galianabujanda@wyss.harvard.edu), N. Karavas (e-mail: nkaravas@seas.harvard.edu), Y. M. Zhou (e-mail: yumengzhou@seas.harvard.edu), C. Walsh (phone: 617-496-7128, e-mail: walsh@seas.harvard.edu) are with the John A. Paulson School of Engineering and Applied Science and the Wyss Institute for Biologically Inspired Engineering, Harvard University, Cambridge, MA 02138 USA

Corresponding author: C. J. Walsh

guiding suit architecture design, controller development and biomechanical and physiological studies [20]–[23], [27]. Those results of our research have also helped guide the design of our fully autonomous portable systems [28], [29].

While a number of groups have now shown exciting metabolic reductions with both autonomous and tethered wearable robots, it is well accepted that there remains scope to better optimize the assistive profiles for wearer to achieve maximum benefit with these systems. Already, many researchers have worked on investigating the effects on changes in control parameters (e.g. timing and magnitude of the assistance) on biomechanical and physiological objectives to better understand the human-robot interaction landscapes [16], [23], [24], [30], [31]. A major challenge in the field to date has been the large variability in response across subjects in various studies and so recently there is also growing interest in applying optimization techniques to automatically tune control parameters for individual wearers to minimize or maximize some objective function [32], where needs the actuation system to track the shape of the optimized assistance profile accurately.

Our previous actuation platforms and control approaches provided decent tracking of the key features of the desired force profile within a limited magnitude range under normal walking speed [21], [22]. However, given the growing recognition of the importance of tuning assistance profiles to different individuals and initializing our research on assisting jogging, we set to create an upgraded tethered actuation system and control approach to enable force tracking across a range of different profiles that can be modified instantaneously under normal walking and jogging speed.

In this paper, we present a more powerful actuation platform and a switching admittance-position control approach. The expandable off-board system consists of a two degree of freedom modular actuation unit that can generate assistive forces delivered through our soft exosuit under normal walking or jogging speed. The new control approach was developed to utilize the advantages of both admittance and position control to perform accurate force tracking and cable slack management. In particular, three feedforward models (FFMs) are studied and added to the admittance control to compensate for variability of individual kinematics, nonlinear hip exosuit stiffness and improve the actuator performances under a varied cable force and speed environment. Results of human subject experiments demonstrated the importance of the FFMs; they enabled the accurate assistive profile tracking of various shapes, magnitudes, and timings with soft exosuit for walking and jogging.

II. Soft Exosuit

As an initial exploration, we chose to validate our actuation system and control approach with the mono-articular hip exosuit due to its simplicity as shown in Figure 2. The textile components of the hip exosuit consisted of a spandex base layer, a waist belt, two thigh braces and two elastic straps for IMUs. The waist belt and thigh braces were constructed with a woven fabric with reinforcement webbing, and neoprene was added to the waist belt to better spread the pressure around the iliac crest of the wearer, which was previously described in [21], [23], [28]. The IMU (VN-100 Rugged IMU, Vectornav Technologies, TX, USA) is secured by elastic straps on the anterior part of the thigh and measures the thigh angle that is used for gait cycle (GC) event detection.

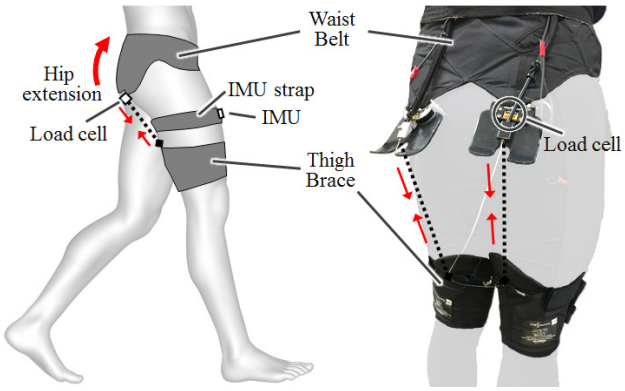

Figure 2. Diagram (left) and photo (right) of a person wearing the hip exosuit with sensor implementation.

TABLE I. DESIGN REQUIREMENTS OF ACTUATION SYSTEM FROM BIOLOGICAL DATA

	Walking (1.25 m/s)		Jogging (2.3 m/s)	
	Ankle	Hip	Ankle	Hip
Range of joint motion (deg)	27	29	44	44
Max. joint speed (rad/s)	2.8	2.5	6.7	4.5
Max. joint moment (Nm)	130	104	75	29
Exosuit moment arm (m)	0.1	0.15	0.1	0.15
Cable travel length (m)	0.14	0.15	0.14	0.17
Actuator minimum speed (m/s)	2.8	1.3	3.1	2.3
Actuator peak force (N)	1300	693	750	192

Two Bowden cable anchor points are at the bottom of the back side of the waist belt and the top center of the thigh brace on the back of the leg respectively. The load cell (LSB200, Futek Advanced Sensor Technology Inc., CA, USA) is integrated in the aluminum anchor point attachment piece to measure the cable force. When the actuator pulls the inner cable, the soft exosuit generates a force that in parallel with the wearer's hip extension muscles by shortening the distance between the two anchor points. More details of suit structure and modeling can be found in [21], [23], [28].

III. Hardware Implementation

A. Biological Requirements

To be capable of replicating the full biological ankle and hip joint moments of walking and 30% of jogging, we calculated our actuation specifications based on data in [33], [34], as shown in Table I. The required assistive torque for ankle and hip are around 130 Nm and 104 Nm respectively for an 80 kg subject walking at 1.25 m/s, and 75 Nm and 29 Nm for 30% of biological ankle and hip joint moment of jogging at 2.3 m/s. The average angular speed of hip and ankle joint reach up to 2.8 rad/s and 2.5 rad/s for walking, 6.7 rad/s and 4.5 rad/s for jogging respectively. To translate torque and rotational motion into cable force $F(t)$ and speed, the moment arm for each joint was estimated based on the design of our current soft exosuit. Using the soft exosuit stiffness model $f_{suit}(F)$ evaluated in Section IV, the minimum required

actuator speed V_{min} is the sum of the cable velocity used to follow the motion of biological joints $V_{motion}(t)$ and the soft exosuit deformation speed with the desired assistive force $\frac{d}{dt}\left(\frac{F(t)}{f_{suit}(F(t))}\right)$. Travel length for cable L_t is the maximum stroke reached when integrating the actuator speed V_{act}. Those relations are also shown in (1) and (2).

$$V_{min} = \max\|V_{act}(t)\| = \max\left\|V_{motion}(t) + \frac{d}{dt}\left(\frac{F(t)}{f_{suit}(F(t))}\right)\right\| \quad (1)$$

$$L_t = \max\left\{\int V_{act}(t)\right\} - \min\left\{\int V_{act}(t)\right\} \quad (2)$$

The biological data and calculated actuator specifications based on (1) and (2) are listed in Table I.

B. Actuation System

The two DOF modular actuator units of the off-board platform are shown in Figure 3. Each DOF has a peak force capability of 1480 N and maximum speed of 3.2 m/s with an 85 V power supply that satisfies the listed biological requirements. Each actuator consists of a customized frameless brushless motor (Allied Motion, Colorado, USA) with a no-load speed of 6122 rpm and a peak torque of 10.87 Nm, a customized 9.25:1 spiroid gear set (ITW Heartland, MN, USA) and a 45 mm radius pulley. The pulley groove is designed to be able to wrap the inner Bowden cable 1.5 times around the pulley, allowing 420 mm of cable travel. As a safety feature, a mechanical slip clutch is located between the spiroid gear and pulley. Once the cable force exceeds the set threshold, the output pulley will start to slip. One encoder (360 cnt/rev, AS5134, Ams, Premstaetten, Austria) is mounted on the back of our customized motor. It measures the position and velocity of the motor. Four cooling fans (L034625, Delta electronics, Taiwan) are installed in front of the heat sink on the actuator bottom case.

Bowden cables are used to transmit the force from the actuation system to the hip exosuit as shown in Figure 1. The cable sheath of the actuator side connects to the pulley cover and inner cable attaches to the pulley as shown in Figure 3. When the motor rotates, the actuator can either pull in the inner cable to generate a force on the hip exosuit or push the cable out so it can go slack.

C. Control System Architecture

The electronics hardware has a three-layer configuration for the control system architecture: real time target machine (top layer), microprocessor (middle layer), and servomotor driver (bottom layer). By leveraging a previously developed integrated circuit board including microprocessor and servomotor driver [29] and the control structure of previous multi-joint actuation platform [20], only communication between layers is required to close the control loop across all layers. CAN Communication was selected to satisfy the 1 kHz control loop rate requirement for a simpler implementation compared to Ethercat.

In the top layer, a dell precision T3500 computer is configured as the real time target machine that runs Matlab Simulink for the control implementation. A PCI interface card for CAN (CAN-AC PCI, Softing AG, Haar, Germany) is installed on this computer to acquire sensor signals and send desired current to servomotor driver through the microprocessor. All sensors and actuator signals including load cell, IMU, actuator encoders command motor current and measured motor current are all logged on the real time target machine at the control loop frequency. An Arduino Due is selected as the microprocessor in the middle layer. It acts as a signal hub between real time target machine and servomotor driver while protecting the system from undesired behavior of the actuator due to anomalous errors of signals from real time target machine. In the bottom layer, Gold Twitter (Elmo Motion Control Ltd, Israel) with 55V maximum supply voltage and 60 A peak current is selected as the current servomotor driver. It tracks the checked current command from the microprocessor to drive the actuator at the desired speed and stiffness. With this control system structure, it keeps the possibility to make this actuation modular to be a self-contained actuation system without an external real time target machine similar to the off-board system in [22].

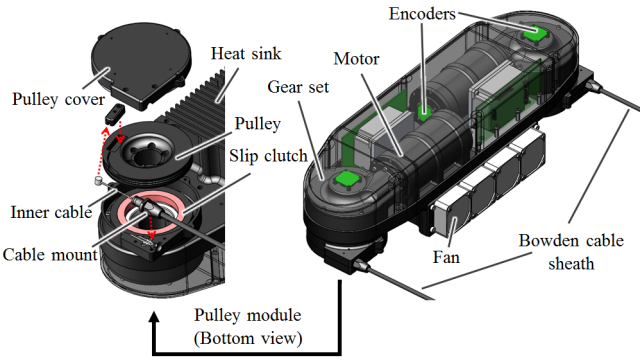

Figure 3. 3-D CAD diagram of actuation system.

IV. System Modeling

To achieve accurate force tracking on a moving object through a soft interface, we need a high bandwidth control system. Feedforward ideas are shown to lead an increase in the effective bandwidth of a close-loop control and an improvement on tracking performance in previous studies [35], [36]. In this section, we present accurate models of suit stiffness, thigh motion, and actuator transmission. These models are integrated into our control architecture as feed forward models that significantly improved the force tracking performance of our actuation system. The detailed implementation of each FFM is described in Section V.

A. Suit stiffness model

The suit stiffness model is intended to enable the controller to compensate for the nonlinear deformation in the hip exosuit when assistance force is generated. Using desired reference force as the input to calculate the required cable position is the purpose of the suit stiffness model. For the model derivation, we measured the stiffness of waist and thigh garment for three health male subjects (30 ± 1 years old; 70 ± 7 kg; 172 ± 8 cm) by capturing the relation between changed cable length and resulted cable force while mimic actuation at the hip joint. The subjects were asked to stand in a pose with feet 50 cm apart in a pose close to that at 13% GC, which is close to when force was maximally applied to hip extension in our previous work

[21], [27], [28]. In each trial, the actuator was commanded to generate 250N peak force under a constant velocity around 0.06m/s and release the cable under the same speed. Ten cycles of cable pulling and releasing are recorded with each subject. The results of the measurement are shown in Figure 4. The color dotted lines are the raw data from all three subjects. The black line is the fitted model with a logarithmic function shown as (3). F is the cable force and l_s is the required cable position.

$$l_s = C_{s1}\ln(C_{s2}F + 1) \tag{3}$$

B. Thigh motion model

The thigh motion model is designed to compensate the disturbances brought by the thigh motion while delivering assistance during the walking and jogging. To minimize this disturbance, we try to estimate the needed cable length for different thigh angles measured by the IMU. To model this, we conducted experiments with same subjects who participated in the suit stiffness test. Both IMU signals on the thigh and the cable position from the motor encoder were recorded when the subject swing the corresponding leg back and forth slowly under a constant 15N cable pre-tension for ten cycles. The measurement results are in Figure 5. The color dotted lines are the raw data from all three subjects. The black line is the fitted model with linear function as (4). θ_t is the IMU angle, where 0 is the neutral standing position, negative angle represents hip flexion and positive angle represents hip extension. l_t is the required cable position.

$$l_t = C_t\theta_t \tag{4}$$

C. Actuator transmission model

The actuator transmission model gives estimations of the required motor current to the servomotor driver under different cable forces. With accurate current estimation, it decreases the phase delay of the force tracking. It uses the desired cable forces, cable velocity and the moment inertia and friction effects of the mechanical components to capture the actuator transmission behavior during actuation.

The model is written as $f_a(F_{cable}, V_{cable})$, which is a function of the cable force F_{cable} and speed V_{cable} as (5).

$$\begin{aligned} I_m &= f_a(F_{cable}, V_{cable}) \\ &= \frac{\frac{FD_p}{2N} + \left(J_r + J_{pg} + \frac{J_{rg} + J_p}{N^2}\right)\frac{2N\dot{V}}{D_p}}{K_t\eta_{cable}\eta_{gear}} + C_v\frac{2NV}{K_tD_p} \end{aligned} \tag{5}$$

where η_{cable} and η_{gear} are the efficiency of cable sheath and gear, respectively. C_v is the viscous friction coefficient of overall mechanical components. D_p and N are the pulley diameter and gear ratio, respectively. J_r, J_{pg}, J_{rg} and J_p are the moment inertia of rotor, pinion gear, ring gear, and pulley, respectively. K_t is the motor torque constant. These coefficients are calculated based on the technical data sheet ($\eta_{gear}, N, J_r, J_{pg}, J_{rg}, K_t$), 3-D CAD model ($D_p, J_p$) and estimations by comparing measured and estimated motor currents (η_{cable}, C_v). The η_{cable} is estimated as a constant without considering bending angle effect of the cable sheath.

To validate the actuator transmission model, we fed the model with measured cable force and cable velocity to calculate the estimated current. Then we compared the estimated current with the measured current during assistive walking and jogging conditions. One example of the estimated current and measured current are shown in Figure 6 for two continuous walking steps. The root mean square error (RMS-E) between measured and estimated current is within 3.15A, which is 5.9% of measured peak current.

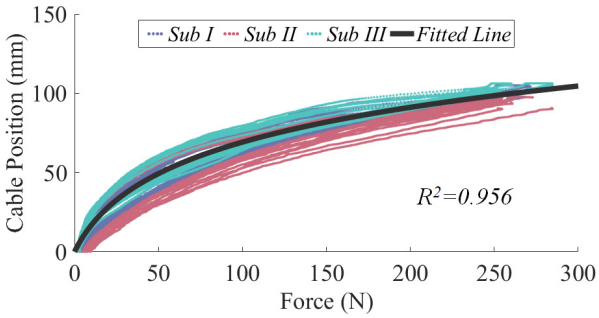

Figure 4. Relation between changed cable length and resulted cable force to calculate suit stiffness model.

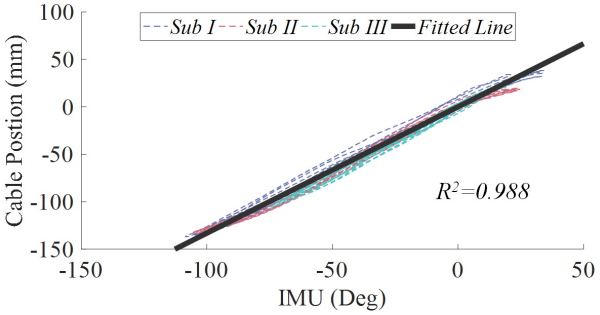

Figure 5. Relation between changed cable length and thigh angle to calculate thigh motion model.

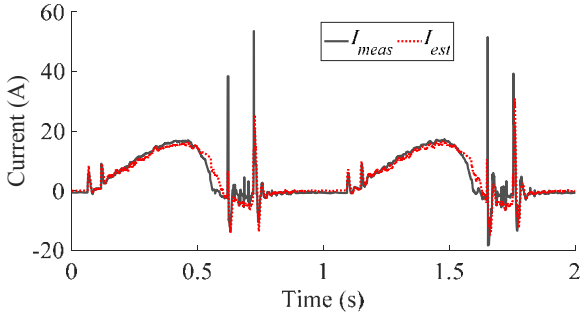

Figure 6. Verification of actuator transmission model by comparing measured and estimated motor currents.

V. Control

A. Gait Event Estimation Using IMU

The IMU attached to the front of each thigh measures the thigh angle in the sagittal plane and a gait detection algorithm identifies the first positive thigh angle peak (corresponding to maximum hip flexion angle) after a negative thigh angle peak (corresponding to maximum hip extension angle) as the maximum hip flexion point. Stride time was measured as the time between two consecutive maximum hip flexion events. The expected duration of the current stride time is estimated from the average of the previous two strides. It is worth noting

that the gait percentage axes for the plots shown in this paper are segmented by the maximum hip flexion. Forces shown in Figure 10 and Figure 11 are shifted to 10% and 20% to the left to make 0% as heel strike based on the maximum hip flexion timing are 90% and 80% GC on average for walking and jogging respectively [21], [23], [37].

B. Switching Admittance-Position Control

It is important to minimize any cable tension during the non-assistive phase with this uni-directional actuation approach. In order to achieve this along with accurate force profile tracking, a switching admittance-position controller based on the GC, similar to the control method described in [38], [39], was implemented to utilize the advantages of both admittance and position controllers in Figure 7 and Figure 8 respectively. The controller is switched to admittance control during assistive phase and it changes back to position control to push the cable out to slack during non-assistive phase.

Admittance control with feedforward models (FFMs) for tracking assistive profile: The admittance controller structure used in this paper is comprised of a cascade-like controller including an inner velocity loop and an outer admittance loop with FFMs as Figure 7. The velocity and force signals are obtained from the encoder in the actuation system and load cell on the hip exosuit.

The virtual admittance in the outer admittance control loop transforms a force error into a desired velocity that is then sent to the inner velocity control loop as feedback term. The admittance equation is defined in the Laplace domain as (6)

$$\mathrm{Y} = \frac{V_d^{fb}}{F_e} = \frac{1}{M_v \cdot s + C_v} \tag{6}$$

where M_v, C_v, V_d^{fb}, F_e, and Y define the virtual inertia, damping, desired cable velocity of feedback term, local assistive force and virtual admittance respectively. The control parameter of M_v and C_v are selected experimentally similar to [20].

Due to the nonlinear soft nature of exosuit and the disturbances from the thigh motions and the varied shape of desired cable force, the actuation platform does not show decent tracking performance with general admittance control. To overcome these limitations, we implemented the suit stiffness and thigh motion models as (3) and (4) in the outer admittance loop as FFMs as shown in (7).

$$V_d^{ff} = \frac{d}{dt}(l_s + l_t) = \frac{C_{s1}C_{s2}}{C_{s2}F_d + 1} + C_t\dot{\theta}_t \tag{7}$$

where V_d^{ff} and F_d define the feedforward term of desired cable velocity and the desired assistive force respectively.

The velocity controller in the inner velocity control loop transforms a velocity error into a desired current that is then sent to the actuator system. The velocity controller use a proportional-integral-derivative (PID) control form. We implemented the actuator transmission model in the velocity control loop as FFM as shown in (8) to enable faster velocity tracking by giving an estimation of the required motor current to the servomotor driver.

$$I_d^{ff} = f_a(F_d, V_d) \tag{8}$$

where I_d^{ff} and f_a define the feedforward term of the desired motor current and the actuator transmission model as (5), respectively.

Position control for slack management: The position controller structure is comprised of two-cascading loops

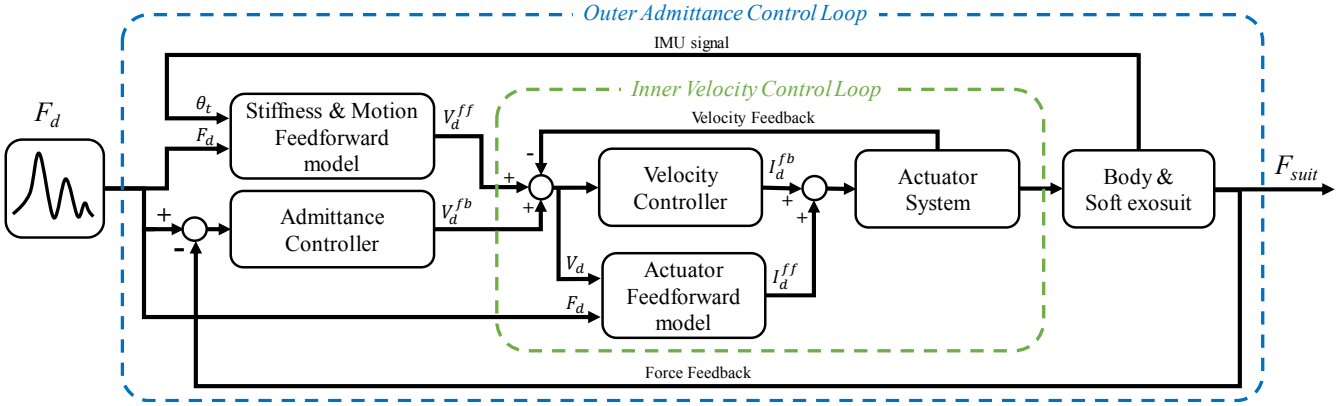

Figure 7. Schematic of admittance control with feedforward models.

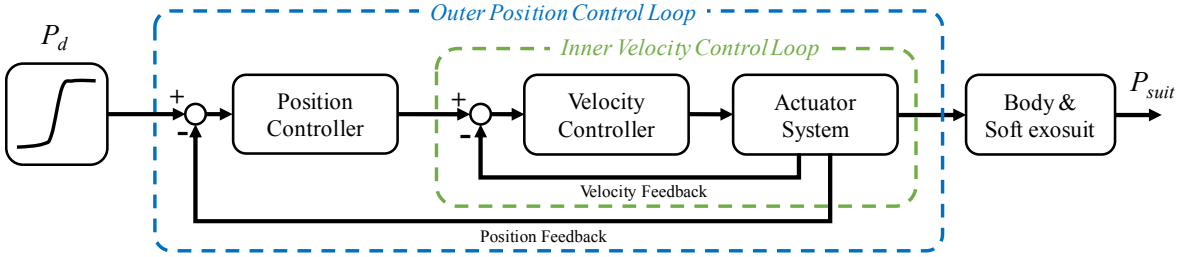

Figure 8. Schematic of position control.

including the outer position loop and the inner velocity loop as Figure 8. With the cascading structure, the controller improves the stiffness and robustness from high-frequency disturbances comparing using a position loop on its own. Both position and velocity controllers in each loop use a proportional-integral-derivative (PID) control form.

VI. System Validation

A. Bandwidth experiment

To evaluate the force tracking performance with or without FFMs, we evaluated the system bandwidth by commanding sinusoidal sweep force signals (from 1 to 30 Hz) with a cable magnitude of 100 N (peak to peak 200 N) for both conditions. The subject was asked to stand in the same posture as described in the suit stiffness test.

The Bode plot of the system with force controller are generated using the Fourier transform of desired and measured signals as Figure 9. Bandwidth was calculated as the lesser of the -3 dB cutoff frequency. The results demonstrate that the force control with FFM show a bandwidth of 19.6 Hz with a phase margin of -119°, demonstrating higher performance compared to our previous actuation system [20]. But without FFM, the force control only shows a bandwidth of 8.3 Hz with a phase margin of -53°. It is helpful to improve the bandwidth which is highly related to the force tracking performance.

B. Human subject experiment

A pilot test was performed with three subjects to evaluate the system controllability for hip extension assistance during walking and jogging on a treadmill at 1.25 m/s and 2.3 m/s, respectively. Experiments were performed on the same subjects who participated in the experiments for system modeling. Each subject walked for one minute for each trial wearing the hip exosuit with different commanded hip extension assistance force profiles. Data from the last ten strides for each condition were analyzed and compared.

During walking, the magnitude, shape, and timing of assistive profiles were varied with shapes approximately matching the biological moment of hip joint during unassisted walking at 1.5 m/s [23], [33]. Since the maximum supply voltage of current servomotor driver is currently limited to 55V, our system cannot reach the maximum speed until we upgrade the hardware, thus the evaluation approach was taken for jogging by only varying the magnitudes. The profile shape was designed based on the hip extension moment during jogging at 2 m/s [40]. Both tests for walking and jogging were

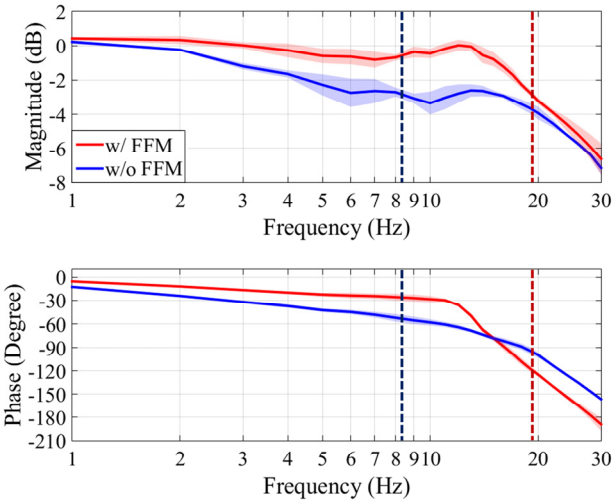

Figure 9. Bandwidth test results of admittance control with or without FFMs.

performed on two conditions, with or without the FFM to compare the effect of the FFM. The admittance gains were tuned as same for both control schemes.

We combine two independent parameterized sinusoidal curves at the peak as the first and second halves to represent a fraction of the simplified biological hip moment. This approach enables the system to quickly change to different magnitude, shape, and timings of assistive profiles by changing parameters of the two sinusoidal curves as shown in (9).

$$F_d(x) = \begin{cases} F_d^p \sin\left(\dfrac{\pi(x - T_d^o)}{2\left(T_d^p - T_d^o\right)}\right), & T_d^o \le x < T_d^p \\ F_d^p \sin\left(\dfrac{\pi\left(x - 2T_d^p + T_d^o\right)}{2\left(T_d^e - T_d^p\right)}\right), & T_d^p \le x < T_d^e \\ 0, \text{ otherwise} \end{cases} \quad (9)$$

where T_d^o, T_d^p, and T_d^e define the desired onset, peak, and end timing of assistive profile in GC respectively, while F_d, F_d^p, and x define the desired assistive force, peak force magnitude, and current GC respectively.

Figure 10(a) shows the results of walking experiments for three different assistive profiles; walk: mag 200N, walk: mag 250N, and walk: mag 300N; with the desired magnitudes (F_d^p)

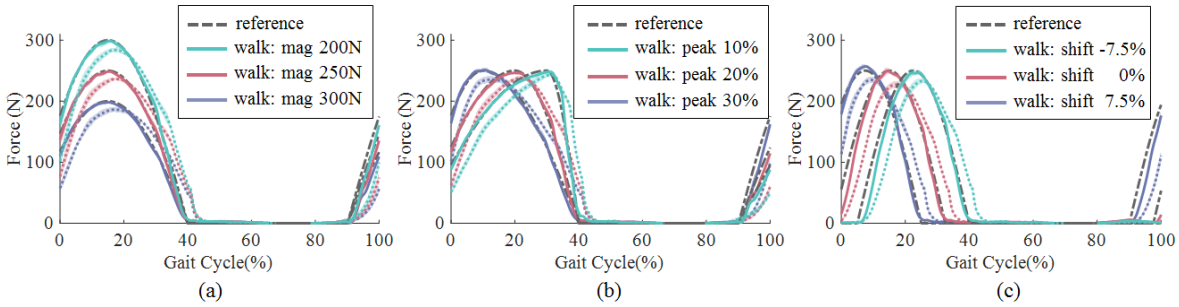

Figure 10. Overlapped tracking results of assistive profiles for walking in three types of experiment: difference in (a) magnitude, (b) shape, and (c) timings. The solid and dotted lines are experiment results on same condition with and without the FFMs, respectively. The shaded areas are standard deviations of measured signals.

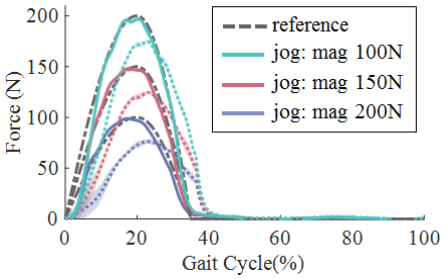

Figure 11. Overlapped tracking results of assistive profiles for jogging in difference magnitudes. The solid and dotted lines are experiment results on same condition with and without the FFMs, respectively. The shaded areas are standard deviations of measured signals.

of 200 N, 250 N, and 300 N with the same timing of onset, peak, and end, which are 90%, 15%, 40%, respectively. To show the tracking performance of the peak magnitudes, the peak value of the measured assistive profile is selected as the representative index. Average-step measured peak force (F_m^p AVG) of assistive profile are analyzed for experiment results with or without the FFMs as shown in Table II. The tracking error of average-step measured peak force of assistive profile with FFMs is within 2.0 N through all the varied magnitude conditions, compared to 16.1 N without FFMs.

Figure 10(b) shows the test results of walking experiments for tracking three different assistive profile shapes walk: peak 10%, walk: peak 20%, walk: peak 30% with different peak timing of 10%, 20%, and 30% in GC while keeping same onset and end timings of 90% and 40%, and magnitude of 250 N. RMS-E of the desired and measured assistive profiles are analyzed to show the overall shape differences. Average-step RMS-E (RMS-E AVG) of the assistive profiles for experiment results with or without the FFMs are shown in Table III. The average-step RMS-E of assistive profile with FFMs is within 8.4 N, which is 3.4% of measured peak force (% F_m^p) through all varied shape conditions, compared to 29.5 N without FFMs.

Figure 10(c) shows the test results of walking experiments for three different shifted assistive profiles with same magnitude of 250N; walk: shift -7.5%, walk: shift 0%, and walk: shift 7.5%; having onset, peak, and end timings as walk: shift -7.5% = (90%, 7.5%, 25%), walk: shift 0%= (97.5%, 15%, 32.5%), and walk: shift 7.5%= (5%, 22.5%, 40%), respectively. walk: shift -7.5% and +7.5% is shifted ±7.5% based on walk: shift 0%. As a representative index, the peak timing of measured assistive profile, which largely represents the tracking performance in terms of timing, is analyzed. Average-step measured peak timing (T_m^p AVG) with or without the FFMs are shown in as Table IV. The tracking error of average-step measured peak timings with FFMs is below 1.8% in GC through all varied timing conditions, compared to 2.8% without FFMs.

Figure 11 shows the results of jogging experiments for three different assistive profiles; jog: mag 100N, jog: mag 150N, and jog: mag 200N; with the desired magnitudes (F_d^p) of 100 N, 150 N, and 200 N with the same timing of onset, peak, and end, which are 0%, 20%, 35%, respectively. To quantify the tracking performance, the peak value of the measured assistive profile is selected as the representative index. Average-step measured peak force (F_m^p AVG) values with and without the FFMs as shown in Table V. The tracking

TABLE II. DESIRED AND MEASURED PEAK FORCE OF DIFFERENT MAGNITUDES OF WALKING EXPERIMENTS

	F_d^p	F_m^p AVG w/ FFD	F_m^p AVG w/o FFD
walk: mag 200N	200 N	198.0 N	186.2 N
walk: mag 250N	250 N	248.6 N	236.3 N
walk: mag 300N	300 N	298.4 N	283.9 N

TABLE III. MEASURED RMS-E OF DIFFERENT SHAPES OF WALKING EXPERIMENTS

	w/ FFD		w/o FFD	
	RMS-E AVG	% F_m^p	RMS-E AVG	% F_m^p
walk: peak 10%	8.4 N	3.4%	29.5 N	11.8%
walk: peak 20%	5.4 N	2.2%	28.2 N	11.3%
walk: peak 30%	5.4 N	2.2%	27.1 N	10.8%

TABLE IV. DESIRED AND MEASURED PEAK TIMINGS OF THE SHIFTED PROFILES OF WALKING EXPERIMENTS

	T_d^p	T_m^p AVG w/ FFD	T_m^p AVG w/o FFD
walk: shift -7.5%	7.5%	7.7%	9.3%
walk: shift 0%	15%	14.6%	17.6%
walk: shift 7.5%	22.5%	24.3%	25.3%

TABLE V. DESIRED AND MEASURED PEAK FORCE OF DIFFERENT MAGNITUDES OF JOGGING EXPERIMENTS

	F_d^p	F_m^p AVG w/ FFD	F_m^p AVG w/o FFD
jog: mag 100N	100 N	98.8 N	76.1 N
jog: mag 150N	150 N	147.5 N	124.5 N
jog: mag 200N	200 N	197.0 N	174.6 N

error of average-step measured peak force of assistive profile with FFMs is within 3.0 N through all the varied magnitude conditions, compared to 25.5 N without FFMs.

VII. CONCLUSION

In this paper, we demonstrate accurate force profile tracking of various shapes, magnitudes, and timings for soft exosuits under normal walking and jogging speed using a powerful off-board actuation platform and an improved control approach. In particular, the use of FFMs that account for disturbances from thigh motion, nonlinear hip human-exosuit stiffness and actuator transmission model largely improved the controller's bandwidth and tracking performances. The actuation system enables us to explore how to individualize assistance profiles to achieve higher metabolic reduction for different wearers during walking and jogging.

In future work, we plan to upgrade the control architecture with adaptive control approach, which updates the control parameters according to different walking kinematics and suit-human stiffness across individuals. In addition, we plan to explore more diverse assisting jogging with the methods presented.

ACKNOWLEDGMENT

The authors thank Maria Athanassiu, Adam Couture, Asa Eckert-Erdheim and Diana Wagner for their contributions to the development of the hardware used in this study.

REFERENCES

[1] A. Esquenazi, M. Talaty, A. Packel, and M. Saulino, "The ReWalk Powered Exoskeleton to Restore Ambulatory Function to Individuals with Thoracic-Level Motor-Complete Spinal Cord Injury," *Am. J. Phys. Med. Rehabil.*, vol. 91, no. 11, pp. 911–921, 2012.

[2] P. D. Neuhaus, J. H. Noorden, T. J. Craig, T. Torres, J. Kirschbaum, and J. E. Pratt, "Design and evaluation of Mina: A robotic orthosis for paraplegics," *in Proc. IEEE Int. Conf. Rehabil. Robot. (ICORR)*, Jun, 2011.

[3] B. J. Ruthenberg, N. A. Wasylewski, and J. E. Beard, "An experimental device for investigating the force and power requirements of a powered gait orthosis," *J. Rehabil. Res. Dev.*, vol. 34, no. 2, pp. 203–213, 1997.

[4] Y. Ohta, H. Yano, R. Suzuki, M. Yoshida, N. Kawashima, and K. Nakazawa, "A two-degree-of-freedom motor-powered gait orthosis for spinal cord injury patients," *Proc. Inst. Mech. Eng. H.*, vol. 221, no. 6, pp. 629–639, 2007.

[5] B. Koopman, E. H. F. Van Asseldonk, and H. Van Der Kooij, "Estimation of human hip and knee multi-joint dynamics using the lopes gait trainer," *IEEE Trans. Robot.* vol. 32, no. 4, pp. 920–932, 2016.

[6] J. Hu, Y. J. Lim, Y. Ding, D. Paluska, A. Solochek, D. Laffery, P. Bonato, and R. Marchessault, "An advanced rehabilitation robotic system for augmenting healthcare," *in Proc. Annu. Int. Conf. IEEE Eng. Med. Biol. Soc. (EMBS)*, pp. 2073–2076, Aug, 2011.

[7] D. Zanotto, P. Stegall, and S. Agrawal, "ALEX III: A novel robotic platform with 12 DOFs for human gait training," *in Proc. IEEE Int. Conf. Robot. Autom.* (*ICRA)*, pp. 3914–3919, May, 2013.

[8] C. J. Walsh, K. Endo, and H. Herr, "A Quasi-Passive Leg Exoskeleton for Load-Carrying Augmentation," *Int. J. Humanoid Robot.*, vol. 4, no. 3, pp. 487–506, 2007.

[9] H. Kazerooni, "The Berkeley Lower Extremity Exoskeleton project," *Springer Tracts Adv. Robot.*, vol. 21, pp. 291–301, 2006.

[10] W. Kim, S. Lee, H. Lee, S. Yu, J. Han, and C. Han, "Development of the heavy load transferring task oriented exoskeleton adapted by lower extremity using qausi-active joints," *in Proc. ICCAS-SICE*, pp. 1353–1358, Aug, 2009.

[11] L. M. Mooney, E. J. Rouse, and H. M. Herr, "Autonomous exoskeleton reduces metabolic cost of human walking during load carriage," *J. Neuroeng. Rehabil.*, vol. 11, no. 80, 2014. (doi: 10.1186/1743-0003-11-80)

[12] A. Schiele, "Ergonomics of exoskeletons: Subjective performance metrics," *in Proc. IEEE/RSJ Int. Conf. Intell. Robot. Syst. (IROS),* pp. 480–485, Oct, 2009.

[13] A. H. A. Stienen, E. E. G. Hekman, F. C. T. van der Helm, and H. van der Kooij, "Self-aligning exoskeleton axes through decoupling of joint rotations and translations," *IEEE Trans. Robot.*, vol. 25, no. 3, pp. 628–633, 2009.

[14] H. Kazerooni, A. Chu, and R. Steger, "That Which Does Not Stabilize, Will Only Make Us Stronger," *Int. J. Rob. Res.*, vol. 26, no. 1, pp. 75–89, 2007.

[15] L. M. Mooney, E. J. Rouse, and H. M. Herr, "Autonomous exoskeleton reduces metabolic cost of walking," *in Proc. Annu. Int. Conf. IEEE Eng. Med. Biol. Soc. (EMBS)*, pp. 3065–3068, Aug, 2014.

[16] S. H. Collins, M. B. Wiggin, and G. S. Sawicki, "Reducing the energy cost of human walking using an unpowered exoskeleton," *Nature*, vol. 522, no. 7555, pp. 212–215, 2015.

[17] K. Seo, J. Lee, Y. Lee, T. Ha, and Y. Shim, "Fully Autonomous Hip Exoskeleton Saves Metabolic Cost of Walking," *in Proc. IEEE Int. Conf. Robot. Autom.* (*ICRA),* pp. 4628–4635, May, 2016.

[18] A. T. Asbeck, R. J. Dyer, A. F. Larusson, and C. J. Walsh, "Biologically-inspired soft exosuit," *in Proc. IEEE Int. Conf. Rehabil. Robot. (ICORR)*, pp. 1-8, Jun, 2013.

[19] A. T. Asbeck, S. M. M. De Rossi , I. Galiana , Y. Ding, and C. J. Walsh, "Stronger, smarter, softer: next-generation wearable robots," *IEEE Robot. Autom. Mag*, vol. 21, no. 4, pp. 22–33, 2014.

[20] Y. Ding, I. Galiana, A. Asbeck, B. Quinlivan, S. M. M. De Rossi, and C. Walsh, "Multi-joint actuation platform for lower extremity soft exosuits," *in Proc. IEEE Int. Conf. Robot. Autom. (ICRA)*, pp. 1327–1334, May, 2014.

[21] Y. Ding, I. Galiana, C. Siviy, F. A. Panizzolo, and C. Walsh, "IMU-based Iterative Control for Hip Extension Assistance with a Soft Exosuit," *in Proc. IEEE Int. Conf. Robot. Autom. (ICRA)*, pp. 3501-3508, May, 2016.

[22] S. Lee, S. Crea, P. Malcolm, I. Galiana, A. Asbeck, and C. Walsh, "Controlling Negative and Positive Power at the Ankle with a Soft Exosuit," in *Proc. IEEE Int. Conf. Robot. Autom. (ICRA),* pp. 3509-3515, May, 2016.

[23] Y. Ding, F. A. Panizzolo, C. J. Siviy, P. Malcolm, I. Galiana, K. G. Holt, and C. J. Walsh, "Effect of timing of hip extension assistance during loaded walking with a soft exosuit," *J. Neuroeng. Rehabil.*, vol. 13, no. 87, 2016. (doi: 10.1186/s12984-016-0196-8)

[24] R. W. Jackson and S. H. Collins, "An experimental comparison of the relative benefits of work and torque assistance in ankle exoskeletons," *J. Appl. Physiol.*, vol. 119, no. 5, pp. 541–557, 2015.

[25] J. R. Koller, D. A. Jacobs, D. P. Ferris, and C. D. Remy, "Learning to walk with an adaptive gain proportional myoelectric controller for a robotic ankle exoskeleton," *J. Neuroeng. Rehabil.*, vol. 12, no. 97, 2015. (doi: 10.1186/s12984-015-0086-5)

[26] S. Huang, J. P. Wensman, and D. P. Ferris, "An Experimental Powered Lower Limb Prosthesis Using Proportional Myoelectric Control," *J. Med. Device.*, vol. 8, no. 2, 2014. (doi: 10.1115/1.4026633)

[27] Y. Ding, I. Galiana, A. T. Asbeck, S. M. M. De Rossi, J. Bae, T. R. Teles Dos Santos, V. Lara de Araujo, S. Lee, K. Holt, and C. J. Walsh, "Biomechanical and physiological evaluation of multi-joint assistance with soft exosuits," *IEEE Trans. Neural Syst. Rehabil. Eng.*, 2016. (doi: 10.1109/TNSRE.2016.2523250)

[28] A. T. Asbeck, K. Schmidt, I. Galiana, and C. J. Walsh, "Multi-joint Soft Exosuit for Gait Assistance," *in Proc. IEEE Int. Conf. Robot. Autom. (ICRA)*, pp. 6197-6204, May, 2015.

[29] F. A. Panizzolo, I. Galiana, A. T. Asbeck, C. Siviy, K. Schmidt, K. G. Holt, and C. J. Walsh, "A biologically-inspired multi-joint soft exosuit that can reduce the energy cost of loaded walking," *J. Transl. Med.*, vol. 13, no. 43, 2015. (doi: 10.1186/s12984-016-0150-9)

[30] P. Malcolm, W. Derave, S. Galle, and D. De Clercq, "A Simple Exoskeleton That Assists Plantarflexion Can Reduce the Metabolic Cost of Human Walking," *PLoS One*, vol. 8, no. 2, e56137, 2013.

[31] M. Wehner, B. Quinlivan, P. M. Aubin, E. Martinez-Villalpando, M. Baumann, L. Stirling, K. Holt, R. Wood, and C. Walsh, "A lightweight soft exosuit for gait assistance," *in Proc. IEEE Int. Conf. Robot. Autom. (ICRA)*, pp. 3362–3369, May, 2013.

[32] J. R. Koller, D. H. Gates, D. P. Ferris, and C. D. Remy, "'Body-in-the-Loop' Optimization of Assistive Robotic Devices: A Validation Study," *Robot. Sci. Syst.*, 2016. (in press)

[33] D. A. Winter, *Biomechanics and motor control of human movement*, John Wiley & Sons, 2009.

[34] A. S. Voloshina and D. P. Ferris, "Biomechanics and energetics of running on uneven terrain," *J. Exp. Biol.*, vol. 218, no. 5, pp. 711–9, 2015.

[35] S. G. Yuen, D. P. Perrin, N. V Vasilyev, P. J. Nido, and R. D. Howe, "Force Tracking With Feed-Forward Motion Estimation for Beating Heart Surgery," *IEEE Trans. Robot.*, vol. 26, no. 5, pp. 888–896, 2010.

[36] G. M. Clayton, S. Tien, K. K. Leang, Q. Zou, and S. Devasia, "A Review of Feedforward Control Approaches in Nanopositioning for High-Speed SPM," *J. Dyn. Syst. Meas. Control*, vol. 131, no. 6, 2009. (doi:10.1115/1.4000158)

[37] T. F. Novacheck, "The biomechanics of running," *Gait and Posture*, vol. 7, pp. 77-95, 1998.

[38] S. H. Collins, M. Kim, T. Chen, and T. Chen, "An ankle-foot prosthesis emulator with control of plantarflexion and inversion-eversion torque," *in Proc. IEEE Int. Conf. Robot. Autom. (ICRA)*, pp. 1210-1216, Jun, 2015.

[39] K. A. Witte, J. Zhang, R. W. Jackson, and S. H. Collins, "Design of Two Lightweight , High-Bandwidth Torque-Controlled Ankle Exoskeletons," *in Proc. IEEE Int. Conf. Robot. Autom. (ICRA),* pp. 1223–1228, May, 2015.

[40] T. K. Uchida, A. Seth, S. Pouya, C. L. Dembia, J. L. Hicks, and S. L. Delp, "Simulating ideal assistive devices to reduce the metabolic cost of running," *PLoS One*, vol. 11, no. 9, pp. 1–19, 2016.